

Interplay of causticity and vorticality within the complex quantum Hamilton-Jacobi formalism

A. S. Sanz* and S. Miret-Artés†

Instituto de Física Fundamental,

Consejo Superior de Investigaciones Científicas,

Serrano 123, 28006 Madrid, Spain

(Dated: December 12, 2018)

Abstract

Interference dynamics is analyzed in the light of the complex quantum Hamilton-Jacobi formalism, using as a working model the collision of two Gaussian wave packets. Though simple, this model nicely shows that interference in quantum scattering processes gives rise to rich dynamics and trajectory topologies in the complex plane, both ruled by two types of singularities: caustics and vortices, where the former are associated with the regime of free wave-packet propagation, and the latter with the collision (interference) process. Furthermore, an unambiguous picture connecting the complex and real frameworks is also provided and discussed.

*Electronic address: asanz@imaff.cfmac.csic.es

†Electronic address: s.miret@imaff.cfmac.csic.es

Realistic simulations of many quantum processes and phenomena of interest —e.g., diffusion, relaxation, transport, dephasing or decoherence in solid state physics, condensed matter or chemical physics— require a detailed knowledge of the time evolution (dynamics) of a relative large number of degrees of freedom. A full quantum-mechanical study of this type of many-body problems via the time-dependent Schrödinger equation (TDSE) results prohibitive computationally. Because of this inconvenience, this kind of problems has become an important and challenging issue in the last years. In particular, many efforts are being devoted to the development of a number of alternative trajectory-based formalisms [1]. The most recent approach considered in the literature, in this direction, is based on using the complex quantum Hamilton-Jacobi (CQHJ) equation, formerly derived by Pauli [2] in 1933 and later on rediscovered by other authors [3, 4, 5, 6, 7, 8, 9]. At a fundamental level, this formulation has been used basically to describe the dynamics associated with stationary states [8, 10, 11, 12], while time-dependent problems have received little attention [13]. However, from a practical (numerical) viewpoint, it has received much more attention [3, 4, 5, 14, 15, 16, 17, 18, 19, 20, 21, 22, 23]. At the moment, the CQHJ equation has been applied to both time-independent (bound states) and time-dependent (scattering) problems, and is actually considered as a potential computational tool to handle relatively large systems. Note that, as also happens with classical waves and fields, solving quantum problems within a complex framework is usually simpler than in a real one.

One of the important problems in quantum trajectory-based methodologies is that of interference dynamics. This characteristic quantum-mechanical process, which is central to many actual research fields in physics and chemistry (e.g., quantum control [24] and quantum information [25]), constitutes however a numerical drawback for such techniques [19, 20, 21, 22, 26], since it introduces the so-called *nodal problem* [26]: the nodal structures associated with interfering amplitudes give rise to numerical instabilities in the calculation of quantum trajectories (and the properties derived from them). In the literature, this issue has been tackled by means of different strategies (see, for instance, Refs. [22, 27, 28]). One of them makes use of the superposition principle, separating the contributions from each partial wave and then taking into account the combined effects of all the contributing partial waves in the end. Nevertheless, despite this strategy may result efficient numerically, from a dynamical viewpoint (i.e., in terms of trajectories) it leads to dramatic consequences: the trajectories associated with a superposition look totally different to those associated

with each separate partial wave [29] due to quantum nonlocality [30]. The purpose of this Letter is to shed some light on this numerical issue by analyzing the topology of complex quantum trajectories and comparing them with their real homologous. The unfolding in the complex space turns relatively simple dynamics in real space into very intricate complex ones, where unexpected and surprising features even for low-dimensional systems are observed. A *vortical dynamics* in the complex configuration space appears as a natural consequence of interference even in 1D, breaking the *causticity regime* characterizing free propagation. Two types of quantum singularities are thus shown to rule the complex dynamics: vortices and caustics. Apart from their intrinsic physical interest, these singularities should also be taken into account when using this formulation for computational purposes, in the design and implementation of numerical algorithms.

For the sake of simplicity, here we consider the 1D CQHJ formulation, although the results can be straightforwardly extended to higher dimensions. Thus, after considering the transformation relation $\Psi(x, t) = e^{i\mathcal{S}(x, t)/\hbar}$, where $\mathcal{S}(x, t)$ is a complex-valued phase depending on the position and time, the TDSE for a particle of mass m in a potential V acquires the form of a Hamilton-Jacobi equation,

$$\frac{\partial \mathcal{S}}{\partial t} + \frac{(\nabla \mathcal{S})^2}{2m} + V - i\hbar \frac{\nabla^2 \mathcal{S}}{2m} = 0. \quad (1)$$

This is the CQHJ equation, where the last term plays the role of a nonlocal, complex quantum potential. Note that, due to the one-to-one correspondence between Ψ and \mathcal{S} (both functions provide exactly the same information), Eq. (1) can also be regarded as the logarithmic form of the TDSE, since its solution (\mathcal{S}) is proportional to $\ln \Psi$. Equation (1) can be further generalized by analytic continuation assuming that both \mathcal{S} and Ψ are complex-valued functions of a complex (space) variable z , i.e., $\bar{\mathcal{S}} \equiv \mathcal{S}(z, t)$ and $\bar{\Psi} \equiv \Psi(z, t)$. Now, analogously to the standard Hamilton-Jacobi formalism, a family of characteristics or trajectories satisfying the motion law (or “guidance” condition) can be defined as

$$\bar{v} \equiv \dot{z} = \frac{\nabla \bar{\mathcal{S}}}{m} = \frac{\hbar}{im} \frac{\nabla \bar{\Psi}}{\bar{\Psi}}, \quad (2)$$

where \bar{v} is, like $\bar{\mathcal{S}}$ and $\bar{\Psi}$, a complex-valued, time-dependent field that depends on the (complex) variable z . Despite this formulation may result inconvenient interpretively, it has been shown [14, 15, 16, 17, 18, 19, 20, 21, 22], however, that numerical algorithms based on it are relatively stable and efficient for low-dimensional systems.

Within a real quantum Hamilton-Jacobi (RQHJ) formulation (the standard Bohmian mechanics) at least two dimensions are necessary in order to observe quantum vorticality [31, 32]. However, as shown below, only one dimension is required to observe the same phenomenon within the CQHJ framework provided quantum interference is involved. The collision of two identical Gaussian wave packets in 1D constitutes an ideal scenario which illustrates fairly well the appearance of vorticality in the complex plane. Before entering into details, first we would like to specify that by collision of two wave packets (either Gaussian or of any other general type) here we mean the problem described by a “one-body” wave function which consists of a wave packet superposition. These wave packets fulfill two conditions initially: (a) they move towards each other and (b) their respective propagation velocities are larger than their spreading rates. With these conditions, after the collision (maximal interference) takes place, two emerging or outgoing wave packets are clearly defined, just like in a classical elastic particle-particle scattering problem. Diffraction-like situations (i.e., those where typical diffraction patterns can be observed after the collision, instead of two emerging wave packets) constitute the opposite case.

The Gaussian wave-packet collision is an analytical problem which, despite its simplicity, could be considered as representative of other more complicated, realistic processes characterized by interference (e.g., scattering problems, diffraction by slits, or quantum control scenarios). As indicated above, this process can be described as

$$\Psi(x, t) = \mathcal{N} [\psi_1(x, t) + \psi_2(x, t)], \quad (3)$$

where \mathcal{N} is the normalizing prefactor. Each wave packet is represented as

$$\psi_j(x, t) = \left(\frac{1}{2\pi\tilde{\sigma}_t^2} \right)^{1/4} \exp \left[-\frac{(x - a_j - v_0^{(j)}t)^2}{4\tilde{\sigma}_t\sigma_0} + \frac{ip_0^{(j)}x}{\hbar} - \frac{iE^{(j)}t}{\hbar} \right], \quad (4)$$

where the complex and real time-dependent spreadings are

$$\tilde{\sigma}_t = \sigma_0 \left(1 + \frac{i\hbar t}{2m\sigma_0^2} \right) \quad (5a)$$

and

$$\sigma_t = \sigma_0 \sqrt{1 + \left(\frac{\hbar t}{2m\sigma_0^2} \right)^2}, \quad (5b)$$

respectively, and the initial width (a real-valued quantity) is given by σ_0 . Regarding the other parameters, a_j is the initial position of the center of the wave packet, and $v_0^{(j)} = p_0^{(j)}/m$

and $E^{(j)}$ are the corresponding velocity and energy, respectively. The space-time contour plots of the probability density, phase and velocity fields associated with Ψ , given by

$$\rho = \Psi^* \Psi, \quad (6a)$$

$$S = \frac{\hbar}{2i} \ln \left(\frac{\Psi}{\Psi^*} \right), \quad (6b)$$

$$v = \dot{x} = \frac{\nabla S}{m}, \quad (6c)$$

respectively, are shown in Fig. 1. It is worth mentioning that Eqs. (6a) and (6b) are transformation relations between the wave field (Ψ and its complex conjugate) and the flow or hydrodynamic fields (ρ, S); the inverse transformation is just given by the polar form of the wave function, $\Psi = \rho^{1/2} e^{iS/\hbar}$, and its complex conjugate. On the other hand, Eq. (6c) arises after the TDSE is recast in a RQHJ form,

$$\frac{\partial S}{\partial t} + \frac{(\nabla S)^2}{2m} + V - \frac{\hbar^2}{2m} \frac{\nabla^2 \rho^{1/2}}{\rho^{1/2}} = 0, \quad (7)$$

plus a continuity (or conservation) equation for the probability density,

$$\frac{\partial \rho}{\partial t} + \nabla \left(\rho \frac{\nabla S}{m} \right) = 0. \quad (8)$$

In order to illustrate the dynamics associated with Ψ , several (real) quantum trajectories $x(t)$ (white solid lines), which are solutions of Eq. (6c), have also been added on each plot. As seen in Fig. 1(a), the interference of the two wave packets leads to the appearance of a nodal structure in ρ , which makes the trajectories to avoid certain space regions. These nodes strongly affect the space-time structures of S and v , as seen in Figs. 1(b) and 1(c), respectively: sudden changes from $-\pi$ (blue) to π (red) around $t_{\max} = 4$ (maximum interference time) in S , and a sharp variation from positive to negative values in v . As clearly noticed from v , the configuration (position) space is divided into two well-defined dynamical regions, where particles will strictly move with either positive (reddish regions) or negative (bluish regions) momentum. Moreover, at $x = 0$, there is a sort of “interface” acting like a (fictitious) barrier, which has a determining influence on the topology of the quantum trajectories: as they start approaching that barrier, they undergo a strong repulsion and bounce backwards. Also, around $x = 0$, v displays a series of local periodic maxima (in the regions with $v > 0$) and minima (for $v < 0$), which become more prominent as time evolves and that, after t_{\max} , they interchange their role (i.e., maxima become minima and

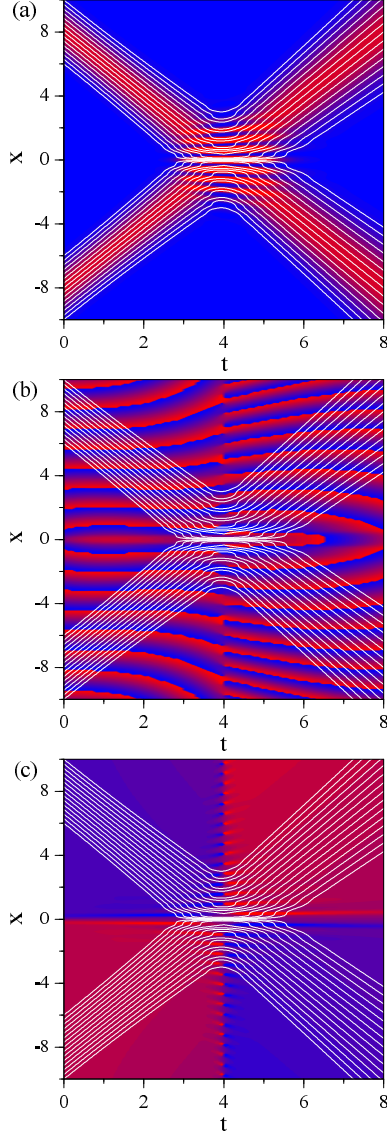


FIG. 1: (Color online.) Space-time contour plots of the probability density (a), phase (b) and velocity (c) fields. The associate flux lines or real quantum trajectories (white solid lines) have been represented in all plots to make easier their understanding. The initial values are $\sigma_0 = 1$, $a_j = \mp 8$, and $v_0^{(j)} = \pm 2$ (with $j = 1, 2$), for a particle with unit mass (arbitrary units are used). The color scale from red to blue ranges from high values of the corresponding field to the lower ones [0 in (a); negative in (b) and (c)].

vice versa). These structures are connected with the nodes of ρ arising after the overlapping of both counter-propagating wave packets. If both wave packets are relatively far apart this effect is so tinny that it is meaningless dynamically (i.e., it does not affect the topology of the quantum trajectories), although it does not mean it does not exist —it persists because

of the initial coherence between ψ_1 and ψ_2 .

In the complex version of the wave packet interference process, the dynamics becomes richer: this 1D problem unfolds into a 2D one on the complex or *Argand* plane, with the dynamics exhibiting more intricate features. Here, we are dealing with complex fields (the wave function and the velocity) which are functions of a complex variable and time. In order to provide a clear picture of the time-evolution of these fields, we will decompose both of them in polar form, i.e.,

$$\mathcal{F}(z, t) = \varrho_{\mathcal{F}}(z, t)e^{i\varphi_{\mathcal{F}}(z, t)}, \quad (9)$$

where $\varrho_{\mathcal{F}}(z, t)$ and $\varphi_{\mathcal{F}}(z, t)$ represent, respectively, the modulus and the phase of the complex field $\mathcal{F}(z, t)$ —in our case, \mathcal{F} stands for $\bar{\Psi}$ and \bar{v} . Thus, in Fig. 2 the contour plots of $\varrho_{\bar{\Psi}}$, $\varrho_{\bar{v}}$ and $\varphi_{\bar{v}}$ are displayed at four different times to illustrate the dynamical evolution in the complex plane. We have not plotted the field $\varphi_{\bar{\Psi}}$ because it is highly oscillating in the space (i.e., on the Argand plane) and time ranges considered, and therefore, very difficult to visualize; instead, we have shown the fields $\varrho_{\bar{v}}$ and $\varphi_{\bar{v}}$, which are related and provide a more clear information. Several remarks are worth stressing. First, as can be inferred from the sequence presented in the upper row of Fig. 2, $\Psi(x, t)$ corresponds to the value of $\bar{\Psi}(z, t)$ along the real axis ($z_r = x$, $z_i = 0$) at the time t . Second, $\bar{\Psi}$ satisfies the normalization condition *only* along the real axis, but not in general on the complex plane. And, third, following the sequence in Fig. 2 (from left to right), we observe that the interference process translates into a 2D anticlockwise rotating dynamics, where at t_{\max} the nodal structure —a set of aligned nodes— just lies on the real axis. At any other time, there is still a nodal alignment, but it is out of the real axis. This explains why, in real space, interference is weaker at any other time than t_{\max} (in other words, the larger $|t - t_{\max}|$, the weaker the interference pattern). Conversely, as \bar{v} shows, the nodal structure remains even for relatively large times ($t \gg t_{\max}$) in the complex space. Taking into account all these observations, we can say that, within this (complex) formulation, the evolution of (real) Ψ can be understood as an “apparent” effect of the evolution of $\bar{\Psi}$ in the complex plane. That is, the value displayed by Ψ at each time can be compared with the frames of a movie tape (which is the role played by $\bar{\Psi}$); each frame is watched only when the corresponding piece of the tape is passing in front of the projector. The sensation of motion then appears when the tape runs in front of the projector (i.e., many frames passing consecutively).

In Fig. 3, the evolution from $t = 0$ to $t = 8$ for four different families of complex

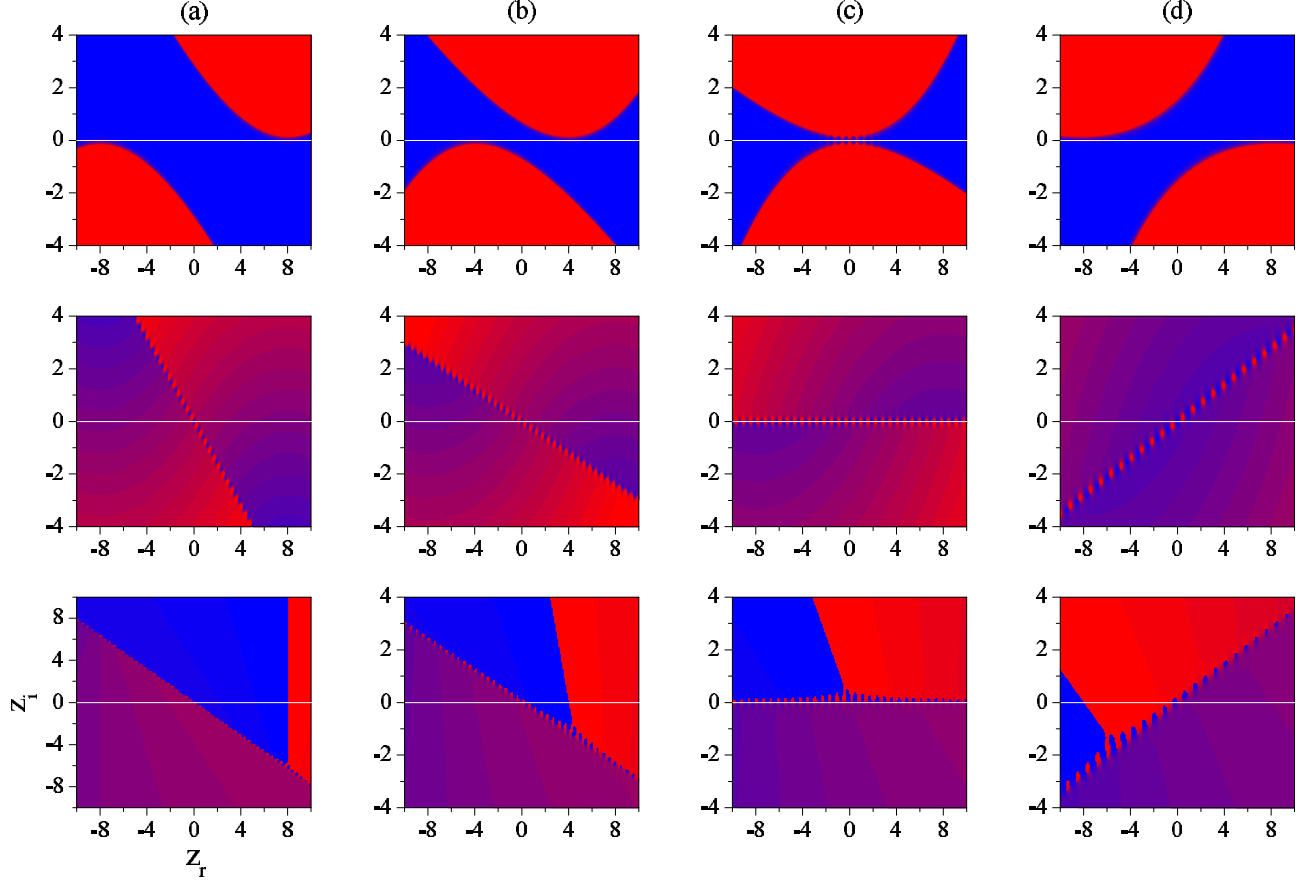


FIG. 2: (Color online.) The three rows, from top to bottom, correspond to the contour plots of $\varrho_{\bar{\psi}}$, $\varrho_{\bar{v}}$ and $\varphi_{\bar{v}}$, respectively, at: (a) $t = 0$, (b) $t = 2$, (c) $t = 4$, and (d) $t = 8$ (arbitrary units are used). The color scale from red to blue ranges from high values of the corresponding field to low ones (0 in the top and middle rows, and negative in the bottom one). The real axis ($z_i = 0$) is denoted by a white solid line in all plots.

trajectories is plotted. Each family represents a set of *isochrones* [14, 15, 16, 19, 20, 21], i.e., all the trajectories belonging to the same family cross the real axis (their imaginary part, z_i , vanishes) at a given time, namely the crossing time t_c (in the cases depicted, at $t_c = 0, 2, 4$ and 8 , respectively). Moreover, in our case, the trajectories of each family have been chosen in such a way that their respective real part coincide with the positions of the real trajectories in Fig. 1 at the time they cross the real axis. Comparing the real and complex trajectory dynamics, it is clear that there is no a simple one-to-one correspondence between both types of trajectories, although they are associated with the same physical problem; real trajectories are not the real part of the complex ones at any time, as suggested elsewhere [10, 11, 12].

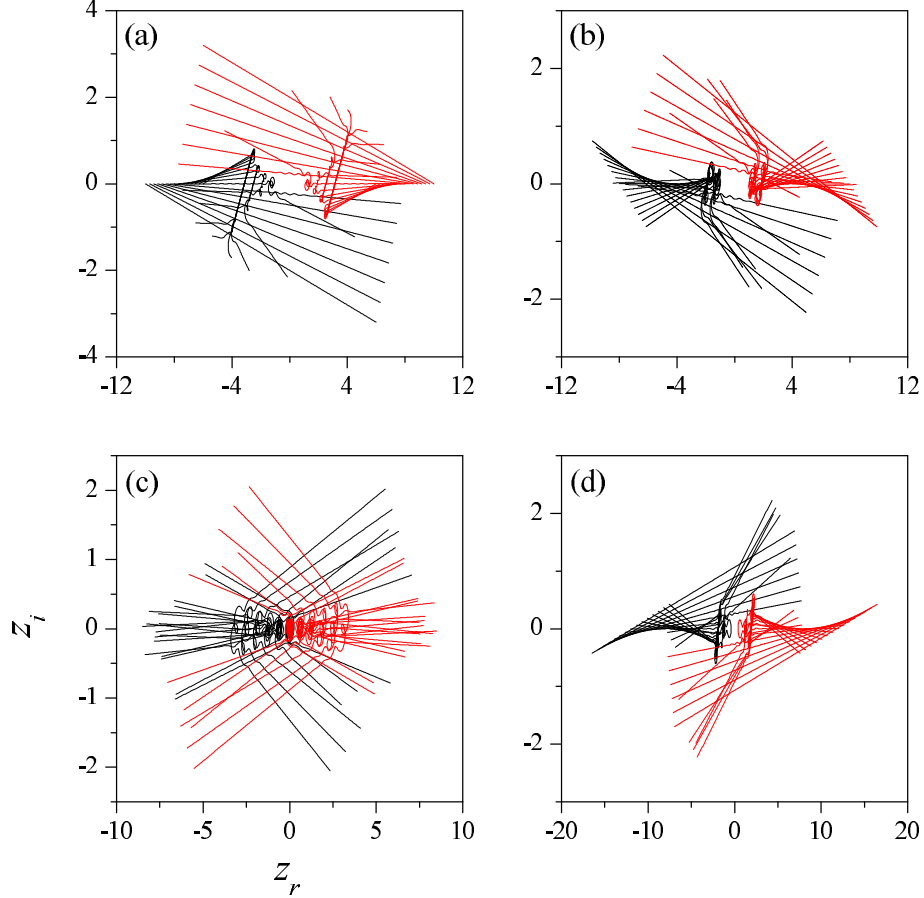


FIG. 3: (Color online.) Isochrones crossing the real axis [$z_i(t_c) = 0$] at: (a) $t_c = 0$, (b) $t_c = 2$, (c) $t_c = 4$, and (d) $t_c = 8$, in accordance with the snapshots shown in Fig. 2 (arbitrary units are used). All the trajectories are propagated from $t = 0$ up to $t = 8$; the crossing points correspond to the same positions reached by the real trajectories in Fig. 1 at the corresponding times. Black and red trajectories are associated with ψ_1 and ψ_2 , respectively.

To establish a connection, one has to consider the movie-based analogy between Ψ and $\bar{\Psi}$ pointed out above and the previous discussion in terms of isochrones. Accordingly, a single real trajectory is made of the crossings of many *different* complex trajectories with the real axis —one crossing for each (real) position at each time. Note that this allows us to define a real trajectory as a family of complex trajectories fulfilling the property that their subsequent crossings (in time) with the real axis generate such a real trajectory. This is, precisely, the reason why when using computational methods based on complex trajectories one needs to consider isochrones to reproduce the corresponding observable [14, 15, 16, 19, 20, 21]. As seen in Fig. 3(c), some of these isochrones can display the effects of a vortical dynamics,

unlike the analogous situation in real configuration space, where vorticity can only be observed in two (or higher) dimensions [31, 32]. Nevertheless, the presence of vortices in complex space can be explained as in a real dynamical framework. In the latter, they appear as a consequence of the presence of nodes in the wave function [31, 32]. In such a case, the rotational of the velocity field does not vanish and trajectories undergo loops around the nodes for some time. Moreover, the motion along closed loops is shown to be quantized, i.e., the circle integral of the action evaluated along a trajectory enclosing a node has a finite, quantized value proportional to the total number of closed loops around the node. Going now to the complex framework, we know that except for a constant in its phase $\varphi_{\bar{\Psi}}$, $\bar{\Psi}$ is uniquely determined, i.e., it remains invariant under a change of phase provided $\varphi'_{\bar{\Psi}} = \varphi_{\bar{\Psi}} + 2n\pi\hbar$, with n being an integer number. Since $\bar{\Psi}$ is a smooth function, discontinuities in its phase ($n \neq 0$) can only occur in nodal regions, where the wave function vanishes and the phase displays “jumps” due to its multivaluedness. These discontinuities give rise to a vortical dynamics, as infers from the circulation of the phase $\varphi_{\bar{\Psi}}$ along a closed path: when $n \neq 0$, \bar{v} is rotational, this leading to the formation of quantum vortices around the nodal regions. The appearance of this dynamics breaks off the causticity regime associated with free wave packet propagation, where (complex) quantum trajectories give rise to the appearance of *caustics*, i.e., curves arising as the envelope of a set of trajectories (all of them tangent to such a curve at different, consecutive times). This can be seen in panels (a), (b) and (d) of Fig. 3. Before and after t_{\max} , the nearly free propagation of ψ_1 and ψ_2 manifests as a sort of causticity regime, which can not be appreciated at all under a strong vortical dynamics, as seen in Fig. 3(c), where this dynamics prevents the isochrones to display the corresponding caustics.

To conclude, from a theoretical and interpretative viewpoint, we have shown that very intricate and rich, complex dynamics can appear provided interference is present even in the case of very simple processes (with simple dynamics in real configuration space). These dynamical behaviors deserve much attention in the design and improvement of numerical techniques based on the CQHJ formalism, since the interplay of vorticity and causticity might become relevant sources of inefficiency when dealing with realistic problems. The knowledge of the complexity involved by the vortical dynamics should be therefore taken into account in the construction and implementation of numerical methods aimed to describe more realistic situations. We would like to note that, rather than being independent, the two

quantum singularities (vortices and caustics) are related through the quantum nonlocality [30]. In this sense, an immediate, natural extension of the study presented here would be multi-interference phenomena, such as the *Talbot effect* [33], which are currently being developed and that constitute an intermediate step before going to more complicated situations, such as surface scattering. It is expected that the information obtained from this type of studies will shed some light on whether working within the CQHJ framework can be further developed and applied to higher-dimensional systems. Up to date (real) trajectory-based methods have been proven to be valuable numerical and interpretative tools to explore this kind of quantum problems; CQHJ methods would further benefit from the advantages of working in the complex space, which have led to well-known numerical simplifications in problems of interest in many other fields of Physics. In particular, the problem we have tackled is a special case due to the dynamical richness mentioned above. However, when dealing with problems with two or higher dimensions, the computational effort of complex trajectories is significantly increased since the dimensionality of the working space is double.

This work has been supported by DGICYT (Spain) under project with reference FIS2007-62006. A.S. Sanz would also like to acknowledge the Spanish Ministry of Education and Science for a “Juan de la Cierva” Contract.

-
- [1] See, for instance: D.A. Micha, I. Burghardt (eds.), *Quantum Dynamics of Complex Molecular Systems*, Springer, Berlin, 2006.
 - [2] W. Pauli, *Die allgemeine Prinzipien der Wellenmechanik*, in *Handbuch der Physik*, H. Geiger and K. Scheel (eds.), Springer-Verlag, Berlin, 1933, Vol. 24, part 1, 2nd ed.
 - [3] R.A. Leacock, M.J. Padgett, *Phys. Rev. Lett.* 50 (1983) 3.
 - [4] R.A. Leacock, M.J. Padgett, *Phys. Rev. D* 28 (1983) 2491.
 - [5] D. Huber, E.J. Heller, R.G. Littlejohn, *J. Chem. Phys.* 89 (1988) 2003.
 - [6] A.S. Sanz, F. Borondo, S. Miret-Artés, *J. Phys.: Condens. Matter* 14 (2002) 6109.
 - [7] R. Guantes, A.S. Sanz, J. Margalef-Roig, S. Miret-Artés, *Surf. Sci. Rep.* 53 (2004) 199.
 - [8] M.V. John, *Found. Phys. Lett.* 15 (2002) 329.
 - [9] D. Tannor, *Introduction to Quantum Mechanics*, University Science Books, Sausalito, CA, 2007.

- [10] See, for instance, this reference and the following two: C.-D. Yang, *Ann. Phys. (N.Y.)* 319 (2005) 399.
- [11] C.-D. Yang, *Ann. Phys. (N.Y.)* 319 (2005) 444.
- [12] C.-D. Yang, *Chaos, Solit. and Fract.* 30 (2006) 342.
- [13] J. Baker-Jarvis, P. Kabos, *Phys. Rev. A* 68 (2003) 042110.
- [14] C.-C. Chou, R.E. Wyatt, *Phys. Rev. E* 74 (2006) 066702.
- [15] C.-C. Chou, R.E. Wyatt, *J. Chem. Phys.* 125 (2006) 174103.
- [16] C.-C. Chou, R.E. Wyatt, *Phys. Rev. A* 76 (2007) 012115.
- [17] B.A. Rowland, R.E. Wyatt, *J. Phys. Chem. A* 111 (2007) 10234.
- [18] R.E. Wyatt, B.A. Rowland, *J. Chem. Phys.* 127 (2007) 044103.
- [19] Y. Goldfarb, I. Degani, D. Tannor, *J. Chem. Phys.* 125 (2006) 231103.
- [20] A.S. Sanz, S. Miret-Artés, *J. Chem. Phys.* 127 (2007) 197101.
- [21] Y. Goldfarb, I. Degani, D. Tannor, *J. Chem. Phys.* 127 (2007) 197102.
- [22] Y. Goldfarb, D. Tannor, *J. Chem. Phys.* 127 (2007) 161101.
- [23] B. Poirier, *Phys. Rev. A* 77 (2008) 022114.
- [24] P.W. Brumer, M. Shapiro, *Principles of the Quantum Control of Molecular Processes*, Wiley-Interscience, Hoboken, NJ, 2003.
- [25] M.A. Nielsen, I.L. Chuang, *Quantum Computation and Quantum Information* Cambridge University Press, Cambridge, 2000.
- [26] R.E. Wyatt, *Quantum Dynamics with Trajectories*, Springer, Berlin, 2005.
- [27] B. Poirier, *J. Chem. Phys.* 121 (2004) 4501.
- [28] D. Babyuk, R.E. Wyatt, *J. Chem. Phys.* 121 (2004) 9230.
- [29] A.S. Sanz, F. Borondo, *Eur. Phys. J. D* (submitted for publication);
e-print arXiv: 0803.2581v1 (quant-ph).
- [30] A.S. Sanz, S. Miret-Artés, *Chem. Phys. Lett.* 445 (2007) 350.
- [31] A.S. Sanz, F. Borondo, S. Miret-Artés, *Phys. Rev. B* 69 (2004) 115413.
- [32] A.S. Sanz, F. Borondo, S. Miret-Artés, *J. Chem. Phys.* 120 (2004) 8794.
- [33] A.S. Sanz, S. Miret-Artés, *J. Chem. Phys.* 126 (2007) 234106.